Interaction Quantification of MTDC Systems Connected with Weak AC Grids

Wanning Zheng, *Member*, *IEEE*, Jiabing Hu, *Senior Member*, *IEEE*, Li Chai, *Member*, *IEEE*, Bing Liu, and Zixia Sang

***Abstract*—The small-signal stability of multi-terminal high voltage direct current (HVDC) systems has become one of the vital issues in modern power systems. Interactions among voltage source converters (VSCs) have a significant impact on the stability of the system. This paper proposes an interaction quantification method based on the self-/en-stabilizing coefficients of the general N-terminal HVDC system with a weak AC network connection. First, we derive the explicit formulae of self-/en-stabilizing coefficients for any N-terminal HVDC system, which can quantify the interactions through different paths analytically. The relation between the self-/en-stabilizing coefficients and the poles of the system can be used to evaluate the impact of the interactions on the system stability effectively. Then, we employ the obtained formulae to analyze the parameter sensitivity and explain how a parameter affects the stability of the system through different paths of interactions. Finally, extensive examples are given to demonstrate the effectiveness of the proposed method.**

***Index Terms*—Interactions, multi-terminal HVDC, self-/en-stabilizing coefficients, small-signal stability.**

NOMENCLATURE

$P_{\rm in}$, $P_{\rm out}$	Active power input and output of VSC.
Q	Reactive power output of VSC.
E, θ	Internal voltage's magnitude and phase.
U_t, θ_t	Terminal voltage magnitude and phase.
U_g, θ_g	Infinite-bus voltage magnitude and phase.
θ_p, ω_p	PLL angular frequency and output angle
$\boldsymbol{I}$	VSC current vector.
$U_{\rm dc}$	DC voltage.
C	DC-capacitance.
$X_{\rm f}$	VSC filter reactance.
X_g	Transmission line reactance in AC system.
R, L	Equivalent resistance and inductance of DC cables.
k_1, k_2	Proportional and integral parameters of the PI controller in DC voltage control.
k_3, k_4	Proportional and integral parameters of the PI controller in a phase-locked loop.
k_5, k_6	Proportional and integral parameters of the PI controller in reactive power control.
k_7, k_8	Proportional and integral parameters of the PI controller in AC current control.
$k_{\rm d}$	Proportional parameter of DC voltage-droop control.

Subscripts

$1, 2, 3, \cdots, N$	Signals in VSCs from 1 to N.
i	Signals in any one of the VSCs.
0	Initial values in a steady-state condition.
d, q	d- and q-axis.
p	PLL-synchronized reference frame.

Manuscript received November 22, 2022; revised January 28, 2023; accepted April 3, 2023. Date of online publication May 3, 2024; date of current version June 22, 2024. This work was supported in part by the National Natural Science Foundation of China under Grant 62173259.

W. N. Zheng and B. Liu are with the Engineering Research Center of Metallurgical Automation and Measurement Technology, Wuhan University of Science and Technology, Wuhan 430081, China.

J. B. Hu is with the State Key Laboratory of Advanced Electromagnetic Engineering and Technology, and School of Electrical and Electronic Engineering, Huazhong University of Science and Technology, Wuhan 430074, China.

L. Chai (corresponding author, email: chaili@zju.edu.cn) is with the College of Control Science and Engineering, Zhejiang University, Hangzhou 310027, China.

Z. X. Sang is with the State Grid Hubei Economic Research Institute, Wuhan 430077, China.

DOI: 10.17775/CSEEJPES.2022.08260

I. INTRODUCTION

A large number of multi-terminal direct current (MTDC) systems have been constructed to integrate and transmit the wind and photovoltaic power in recent years. The small-signal stability of such systems is one of the most important issues, especially when they connect to weak AC grids with a high proportion of renewable energy [1]–[5]. Interactions among the VSCs influence the small-signal stability of the system significantly. Researchers have put a lot of effort into studying the complex interactions and explaining the mechanism of the instability.

The most common method to deal with this problem is the modal analysis method [6]–[9]. Participation factors and sensitivity methods build the relation between the modes, states and the parameters. One can know which states and controllers impact each mode more. It is also possible to analyze the stability of MTDC systems by impedance analysis method, in which VSCs are modeled as impedance in AC and DC sides [10]–[16]. In [17]–[19], the open-loop modal coupling method is proposed to explain the reason for oscillations in MTDC systems. The system is modeled as two subsystems, and the analysis results indicate that the instability risk increases when the two subsystems' modes are close to each other.

However, the above analysis has certain limitations: (i) Interactions among the VSCs are not quantified directly and

analytically. As a result, the available results cannot confirm whether the interactions between the connected VSCs exist, let alone explain whether the interactions are good or bad for the system's stability. (ii) The mechanism of how control parameters, operation points and topologies of networks influence the interactions and further affect the stability is unclear. Although we can obtain some heuristic rules about how the parameters affect the stability from a large number of experiments, there is no guarantee that these rules are applicable to any different cases. Actually, we hope to explore the intrinsic mechanism from the perspective of the interactions among VSCs.

Recently, an interaction quantification method of the MTDC system has been proposed in [20]. Interactions among the VSCs can be quantified by the self-stabilizing coefficient (SSC) and /or stabilizing coefficient (ESC) in the frequency domain. However, the method still has some limitations: (i) The method computes the SSC and ESC based on a signal flow graph, which is too complicated to be applied to the general N-terminal HVDC systems, therefore only suitable for simple three-terminal HVDC systems. (ii) The proposed stability criterion cannot represent the relation between the self-/en-stabilizing coefficients and the poles of the system. (iii) The method did not propose an index to quantify the effect of the parameters on the interactions and stability. (iv) Weak AC grid conditions, which are more likely to cause oscillations in practical situations, are not addressed. The branches of the reactive power are neglected.

This paper proposes a method to quantify the interactions among VSCs of the general N-terminal HVDC system connected with weak AC grids. The main contributions are as follows: (i) We derive explicit formulae of self-/en-stabilizing coefficients for the general N-terminal HVDC system, which can quantify different paths of interactions analytically. (ii) We present a clearer stability criterion that can rigorously explain the relationship between the self-stabilizing coefficients and the poles of the system. By using this criterion, we can evaluate the impact of interactions on system stability through different paths. (iii) We propose the parameter sensitivity of SSC and ESC to quantify the influence of a certain parameter on the stability of the system through different paths of interactions. The results can reveal more insights into the linear process of the interactions among VSCs and provide new ideas for setting and tuning control parameters in MTDC systems.

The rest of the paper is organized as follows. Section II introduces the small-signal model of the general N-terminal MTDC system. Section III presents the quantification method of interactions. The stability criterion and the parameter sensitivity are proposed in Section IV. Case studies are presented in Section V and conclusions are drawn in Section VI.

II. Small-signal Model of an MTDC System with Weak AC Network Connection

Consider the N-terminal HVDC system controlled by I-U DC voltage-droop control, vector control and phase-locked loop (PLL). In the control scheme, I-U DC voltage-droop control is designed to balance the active power flow by controlling the reference DC voltage according to the actual DC current. DC voltage control (DVC), reactive power control (RPC) and AC terminal voltage control (TVC) are the outer loops to manipulate the reference value of d- and q-axis current in a decoupled manner. AC current control (ACC) is cascaded to control the d- and q-axis current. All of them are in a PLL-synchronized reference frame. PI controllers are used in DVC, PLL, RPC, TVC and ACC.

Interactions among multiple VSCs with the above control loops in multiple timescales determine the dynamic behavior of an MTDC system. However, it is very difficult to analyze the actual scenarios directly without any simplification. The whole complex problem can be addressed from two dimensions as shown in Fig. 1. One dimension is different timescales determined by the dynamic response speed of the controllers [23], including the DVC timescale (about 10 Hz) and ACC timescale (about 100 Hz). The other is single VSC or multiple VSCs. In Fig. 1, the complex interactions among multiple VSCs in multiple timescales are shown as a cube (a). Cutting the cube with vertical planes can be divided into the interactions in the DVC timescale (b) and interactions in the ACC timescale (c). When focusing on a single VSC (represented by the horizontal planes in the cube), controllers in multiple timescales interact with each other as well. ACC of a VSC affects the dynamics in the DVC timescale of this VSC first, and then it influences the dynamics of other VSCs in the DVC timescale through the coupling of DC networks. This paper focuses on the interactions among VSCs in the single DVC timescale. We make the following assumptions.

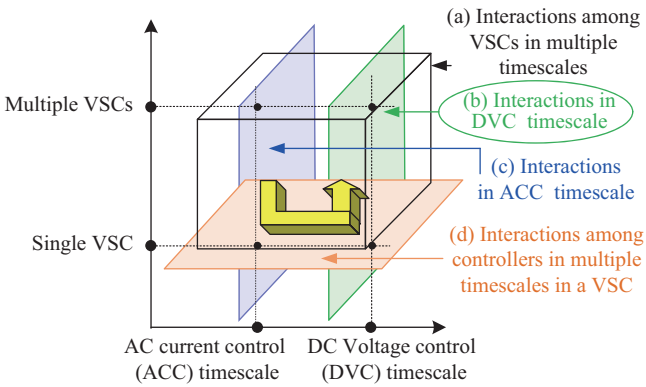

Fig. 1. Illustration of the entire interaction timescales.

- ACC is assumed to be well designed, which means it is quick enough that AC currents can track their reference values instantaneously, and thus the effects of ACC are neglected.
- The effect of dynamics of the inductors and capacitors of the filters and the transmission lines in AC grids is very small. It can be ignored in the DVC timescale since it usually affects the dynamic performance in the ACC timescale.

With these assumptions, a small-signal model of the MTDC system in the DVC timescale is proposed in [24] as shown in Fig. 2. $D_i(s)$ and $G_{mi}(s)$ represent the equivalent damping and inertia of the VSC. $G_{\text{ini}}(s)$ represents the transfer function between the active power input and the phase of the internal

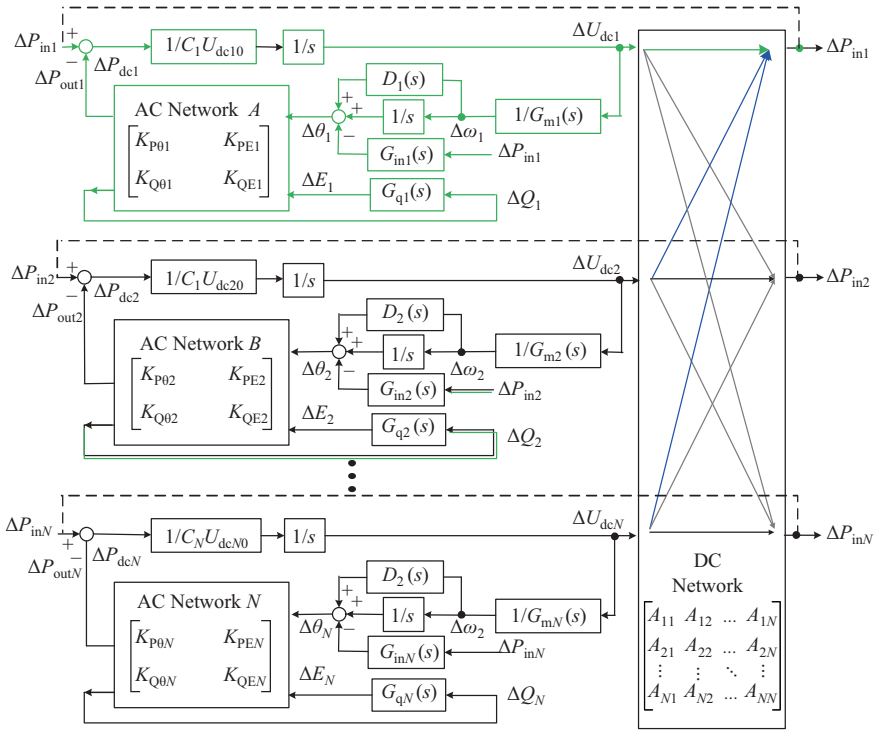

Fig. 2. A small-signal model of an MTDC system in DVC timescale based on the motion equations.

voltage. $G_{\mathrm{qi}}(s)$ represents the transfer function related to reactive power control. Denote the transfer function from DC voltage ΔU_{dci} to the phase of internal voltage $\Delta\theta_i$ as $G_{\mathrm{dci}}(s)$, which can be written as:

$$G_{\mathrm{dci}}(s) = \frac{1 + sD_i(s)}{sG_{mi}(s)} = \frac{\varepsilon_{0i}s^4 + +\varepsilon_{1i}s^3 + \varepsilon_{2i}s^2 + \varepsilon_{3i}s + \varepsilon_{4i}}{s^3} \quad (1)$$

Specific expressions of $G_{\mathrm{ini}}(s)$, $G_{\mathrm{qi}}(s)$ and $\varepsilon_{0i} \sim \varepsilon_{4i}$ are shown in Appendix A.

According to [2], the resistances of the filters and the AC transmission lines are much smaller than the reactance. The steady-state error caused by the resistance is very small and thus, the resistances are neglected in this model. Following the same arguments, many other papers ignored the resistance in the AC network [3], [12], [13], [18], [23]. The availability of the model to describe the dynamic characteristics of a VSC in DVC timescale has been verified by comparing the eigenvalues with the detailed model in [20]. This paper aims to propose an interaction quantification method for the MTDC system. When dealing with interactions in other timescales or the interactions in multiple timescales, we can simply consider other suitable transfer functions.

Two-level VSCs are used in the model. The motivation and reason that we consider the model of two-level VSC instead of MMC converters are threefold. Firstly, two-level VSCs have been widely applied in early HVDC systems [25]–[27], including Estlink system, Valhall offshore system and Nord E. ON. 1 system, etc., although most of the DC transmission and distribution networks constructed use MMC converters now. Secondly, the dynamic performance of an MMC is similar to that of a two-level VSC in the DVC timescale concerned. The difference between an MMC and a two-level VSC includes the circulating current control, unique modulation strategy (e.g., nearest level modulation (NLM)) and discrete capacitors of sub-modules. They mainly influence the dynamics of an MMC in the ACC timescale. Thirdly, the main contribution of this paper is to propose an interaction quantification method for multi-terminal HVDC systems, in which many researchers use the two-level VSC model to analyze the stability of a system with multiple equipment [7], [8], [13], [17], [18].

On the other hand, the MMC model can be derived from a similar motion equation concept as shown by Fig. 2 although transfer functions of $D_i(s)$, $G_{mi}(s)$ and $G_{\mathrm{ini}}(s)$, etc., are different from that of the two-level VSC model. In fact, a small-signal model of an MMC based on the motion equation concept has been proposed in [28]. However, it cannot be used to analyze the interactions in DC grids since it ignores the key active power from other MTDC-linked VSCs in the DC network. It is worthwhile to propose the MMC model for the interaction analysis in the MTDC system by combining the idea of this paper and [28].

I-U DC voltage-droop control, which is a widely accepted and promising control strategy [1], has little influence on the protection schemes. To activate the DC breaker, one method is to measure the DC voltage while measuring the variation rate of the DC voltage or DC current [21], and the other is to set the voltage and current limitations [22]. Although the reference value of DC voltage is not often deliberately changed in practical MTDC systems, it varies smoothly in a small range, which the controller can leverage.

For compact representation, denote

$$\Delta \boldsymbol{P}_{\mathrm{in}} = [\Delta P_{\mathrm{in1}} \quad \Delta P_{\mathrm{in2}} \quad \cdots \quad \Delta P_{\mathrm{inN}}]^{\mathrm{T}}$$

$$\Delta \boldsymbol{P}_{\rm out} = [\Delta P_{\rm out1} \quad \Delta P_{\rm out2} \quad \cdots \quad \Delta P_{\rm outN}]^{\rm T}$$
$$\Delta \boldsymbol{P}_{\rm dc} = [\Delta P_{\rm dc1} \quad \Delta P_{\rm dc2} \quad \cdots \quad \Delta P_{\rm dcN}]^{\rm T}$$
$$\Delta \boldsymbol{U}_{\rm dc} = [\Delta U_{\rm dc1} \quad \Delta U_{\rm dc2} \quad \cdots \quad \Delta U_{\rm dcN}]^{\rm T}$$
$$\Delta \theta = [\Delta \theta_1 \quad \Delta \theta_2 \quad \cdots \quad \Delta \theta_N]^{\rm T}$$
$$\Delta \boldsymbol{E} = [\Delta E_1 \quad \Delta E_2 \quad \cdots \quad \Delta E_N]^{\rm T}$$

Denote $[y_{ij}]$ as the admittance matrix of the DC network. According to the results in [20], power flow in the DC network can be described as:

$$\Delta \boldsymbol{P}_{\rm in} = \boldsymbol{A} \Delta \boldsymbol{U}_{\rm dc} \tag{2}$$

where each element of the matrix

$$\boldsymbol{A}_{ij} \begin{cases} I_{\rm dci0} + y_{ii} U_{\rm dci0}, & i = j \\ y_{ij} U_{\rm dci0}, & i \neq j \end{cases}$$

In AC grids, the active and reactive power of VSC i can be derived as:

$$\begin{bmatrix} \Delta P_{\rm outi} \\ \Delta Q_i \end{bmatrix} = \begin{bmatrix} K_{\rm P\theta i} & K_{\rm PEi} \\ K_{\rm Q\theta i} & K_{\rm QEi} \end{bmatrix} \begin{bmatrix} \Delta \theta_i \\ \Delta E_i \end{bmatrix} \tag{3}$$

where

$$K_{\rm P\theta i} = \frac{E_{i0} U_{\rm gi0} \cos(\theta_{i0} - \theta_{\rm gi0})}{X_{\rm fi} + X_{\rm gi}}$$
$$K_{\rm PEi} = \frac{U_{\rm gi0} \sin(\theta_{i0} - \theta_{\rm gi0})}{X_{\rm fi} + X_{\rm gi}}$$
$$K_{\rm Q\theta i} = \frac{E_{i0} U_{\rm gi0} \sin(\theta_{i0} - \theta_{\rm gi0})}{X_{\rm fi} + X_{\rm gi}}$$
$$K_{\rm QEi} = \frac{2E_{i0} - U_{\rm gi0} \cos(\theta_{i0} - \theta_{\rm gi0})}{X_{\rm fi} + X_{\rm gi}}$$

Based on this small-signal model of the MTDC system in the DVC timescale, interactions among the VSCs can be quantified by analytic expressions based on the SSC and ESCs in the next section.

III. Quantification Method of Interactions

In this section, we will quantify the interactions among the VSCs of the N-terminal HVDC system by SSC and ESC. First, we introduce the definition of SSC and ESC, as well as the principles of decomposing ESC into different terms. Then we elaborate on how to derive SSC and different terms of ESCs of the N-terminal HVDC system.

A. Definition of Self-/En-Stabilizing Coefficients

Consider the i-th VSC of an MTDC system. Its dynamic behavior is not only determined by its dynamic characteristics but also influenced by other VSCs' dynamics through the coupling of the DC network. The unbalanced active power across the DC capacitor of each VSC is the difference between the active power input and output. Combining (2)–(3), the unbalanced active power can be expressed as:

$$\begin{aligned} \Delta P_{\rm dci} &= \Delta P_{\rm ini} - \Delta P_{\rm outi} \\ &= \left(A_{ii} \Delta U_{\rm dci} + \sum_{j \neq i} A_{ij} \Delta U_{\rm dcj} \right) \\ &\quad - (K_{\rm P\theta i} \Delta \theta_i + K_{\rm PEi} \Delta E_i) \end{aligned} \tag{4}$$

Where the part tagged with black lines refers to the dynamics of itself, and the part tagged with blue lines refers to the dynamics affected by other VSCs.

As shown in the small-signal model in Fig. 2, $\Delta U_{\rm dci}$ is the interface of VSC i to the DC network. It is related to the system and the VSCs behind it, and does not respond freely. So we can replace $\Delta \theta_i$, ΔE_i and $\Delta U_{\rm dcj}$ with $\Delta U_{\rm dci}$ according to the transfer functions reflecting the dynamic characteristics of VSCs. Then, (4) can be rewritten as:

$$\Delta P_{\rm dci} = \underbrace{F_{Si}(s) \Delta U_{\rm dci}}_{\Delta P_{Si}} + \underbrace{F_{Ei}(s) \Delta U_{\rm dci}}_{\Delta P_{Ei}} \tag{5}$$

where ΔP_{Si} and ΔP_{Ei} represent the unbalanced active power produced by VSC i and other VSCs. Define $F_{Si}(s)$ as the self-stabilizing coefficient and $F_{Ei}(s)$ as the stabilizing coefficient. $F_{Si}(s)$ reflects the dynamic characteristics related to VSC i, and $F_{Ei}(s)$ reflects the dynamics of all VSCs except VSC i. How to derive $F_{Si}(s)$ and $F_{Ei}(s)$ is one of the main contributions of this paper, which will be presented in the next subsection.

Obviously, ESC has high orders. In order to reflect the interactions through different paths, two principles to decompose ESC into different terms are proposed in [20]. *Principle* 1 is the quantity of VSCs participating in the interactions. *Principle* 2 is the different effects of DC and AC networks. For more details, please refer to [20].

According to the above definitions and principles, we show how to compute SSC and different paths of ESC of the general N-terminal HVDC system in the following subsection.

B. Derivation of the SSC and ESCs of the N-Terminal HVDC System

In this subsection, we first convert the small-signal model in Fig. 2 into a multi-input and multi-output (MIMO) system represented by the transfer function matrix. Then, the SSC and the overall ESC are derived. Finally, we calculate different paths of ESCs according to the two principles.

1) MIMO System Represented by Transfer Function Matrix

In an MTDC system, VSCs transmit the active power and interact with others directly through the DC network. In a strong AC grid, the active and reactive power are almost independent of each other because $K_{\rm PEi}$ and $K_{\rm Q\theta i}$ are very small and can be treated as zero. The reactive power of one VSC would not affect the dynamics of other VSCs through the DC network. In a weak AC grid, however, the active and reactive power couple strongly because $K_{\rm PEi}$ and $K_{\rm Q\theta i}$ are not small enough to be ignored. The reactive power first affects the active power on the AC side and then affects other VSCs through the coupling of the DC network. In other words, the reactive power of one VSC connected with a weak AC grid would affect the dynamic performance of other VSCs although the DC network only transmits the active power. The parameters related to reactive power such as PLL, reactive power control or AC terminal voltage control may play important roles in the interactions among VSCs. Hence, we need to convert the dynamics of the reactive power and the magnitude of internal voltage into the dynamics of the

active power and the phase of internal voltage first. This is the critical difference between the strong and weak AC grids.

Consider the i-th VSC of the system. Based on the small-signal model in Fig. 2, the transfer function from the reactive power to the magnitude of the internal voltage can be written as:

$$\Delta E_i = G_{\mathrm{qi}}(s)\Delta Q_i \tag{6}$$

By expanding (3), the active and reactive power flow in AC networks can be expressed as:

$$\Delta P_{\mathrm{outi}} = K_{\mathrm{P}\theta\mathrm{i}}\Delta\theta_i + K_{\mathrm{PEi}}\Delta E_i \tag{7}$$

$$\Delta Q_i = K_{\mathrm{Q}\theta\mathrm{i}}\Delta\theta_i + K_{\mathrm{QEi}}\Delta E_i \tag{8}$$

Combining (6)–(8), the relationship between $\Delta\theta_i$ and ΔP_{outi} through the coupling of the AC network can be written as:

$$\Delta P_{\mathrm{outi}} = H_i(s)\Delta\theta_i \tag{9}$$

where

$$H_i(s) = K_{\mathrm{P}\theta\mathrm{i}} + \frac{K_{\mathrm{Q}\theta\mathrm{i}}K_{\mathrm{PEi}}G_{\mathrm{qi}}(s)}{1 - K_{\mathrm{QEi}}G_{\mathrm{qi}}(s)} \tag{10}$$

Then, we can represent the small-signal model in the form of the transfer function matrix. The relationship between the unbalanced active power and the DC voltage of VSCs from $1 \sim N$ can be expressed as:

$$\begin{aligned}\Delta\boldsymbol{U}_{\mathrm{dc}} &= \mathrm{diag}\left[\frac{1}{sC_1U_{\mathrm{dc10}}} \quad \cdots \quad \frac{1}{sC_NU_{\mathrm{dcN0}}}\right] \\ &\cdot \Delta\boldsymbol{P}_{\mathrm{dc}} \triangleq \boldsymbol{\Gamma}_1(s)\Delta\boldsymbol{P}_{\mathrm{dc}}\end{aligned} \tag{11}$$

The phase of the internal voltage of VSCs from $1 \sim N$ can be expressed as:

$$\begin{aligned}\Delta\boldsymbol{\theta} &= \mathrm{diag}[G_{\mathrm{dc1}}(s) \quad \cdots \quad G_{\mathrm{dcN}}(s)]\Delta\boldsymbol{U}_{\mathrm{dc}} \\ &\quad - \mathrm{diag}[G_{\mathrm{in1}}(s) \quad \cdots \quad G_{\mathrm{inN}}(s)]\Delta\boldsymbol{P}_{\mathrm{in}} \\ &\triangleq \boldsymbol{\Gamma}_2(s)\Delta\boldsymbol{U}_{\mathrm{dc}} - \boldsymbol{\Gamma}_3(s)\Delta\boldsymbol{P}_{\mathrm{in}}\end{aligned} \tag{12}$$

The active power output of VSCs from $1 \sim N$ can be written as:

$$\Delta\boldsymbol{P}_{\mathrm{out}} = \mathrm{diag}[H_1(s) \quad \cdots \quad H_N(s)]\Delta\boldsymbol{\theta} \triangleq \boldsymbol{\Gamma}_4(s)\Delta\boldsymbol{\theta} \tag{13}$$

By substituting (12) into (13), the active power output can be expressed as:

$$\Delta\boldsymbol{P}_{\mathrm{out}} = \boldsymbol{\Gamma}_4(s)\boldsymbol{\Gamma}_2(s)\Delta\boldsymbol{U}_{\mathrm{dc}} - \boldsymbol{\Gamma}_4(s)\boldsymbol{\Gamma}_3(s)\Delta\boldsymbol{P}_{\mathrm{in}} \tag{14}$$

The unbalanced active power can be calculated as:

$$\Delta\boldsymbol{P}_{\mathrm{dc}} = \Delta\boldsymbol{P}_{\mathrm{in}} - \Delta\boldsymbol{P}_{\mathrm{out}} \tag{15}$$

Combining (2), (14)–(15), the unbalanced active power can be computed by

$$\Delta\boldsymbol{P}_{\mathrm{dc}} = \boldsymbol{L}(s)\Delta\boldsymbol{U}_{\mathrm{dc}} \tag{16}$$

where

$$\boldsymbol{L}(s) = \boldsymbol{A} + \boldsymbol{\Gamma}_3(s)\boldsymbol{\Gamma}_4(s)\boldsymbol{A} - \boldsymbol{\Gamma}_2(s)\boldsymbol{\Gamma}_4(s) \tag{17}$$

Then, the small-signal model in Fig. 2 can be converted into an MIMO model represented by the transfer function matrix as shown in Fig. 3(a), where $\Gamma_1(s)$ is the feedforward channel and $\boldsymbol{L}(s)$ is the feedback channel.

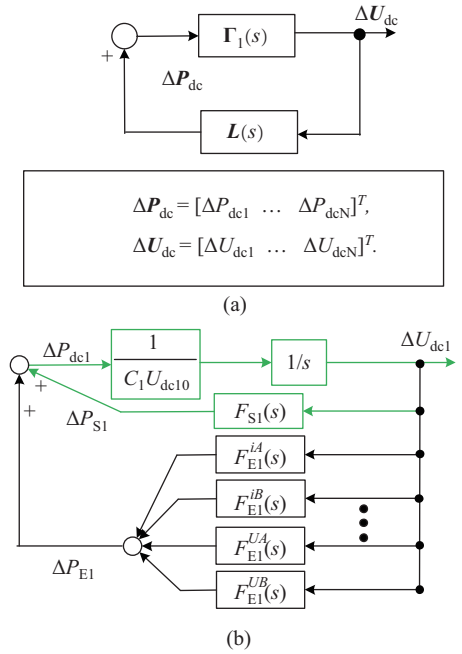

Fig. 3. Small-signal model of an MTDC system with SSC and ESCs. (a) An MIMO model represented by transfer function matrix. (b) The small-signal model with quantification of the interactions.

2) SSC and the Overall ESC

Based on the model in Fig. 3(a), now we can derive the SSC and the overall ESC. Suppose that we focus on VSC 1. Since $\boldsymbol{L}(s)$ consists of the part related to VSC 1 and the part related to other VSCs, then the feedback channel can be expressed as:

$$\Delta P_{\mathrm{dc1}} = L_{11}(s)\Delta U_{\mathrm{dc1}} + [L_{12}(s) \quad \cdots \quad L_{1N}(s)]\begin{bmatrix}\Delta U_{\mathrm{dc2}} \\ \vdots \\ \Delta U_{\mathrm{dcN}}\end{bmatrix} \tag{18}$$

$$\begin{aligned}\begin{bmatrix}\Delta P_{\mathrm{dc2}} \\ \vdots \\ \Delta P_{\mathrm{dcN}}\end{bmatrix} &= \begin{bmatrix}L_{21}(s) \\ \vdots \\ L_{N1}(s)\end{bmatrix}\Delta U_{\mathrm{dc1}} \\ &+ \begin{bmatrix}L_{22}(s) & \cdots & L_{2N}(s) \\ \vdots & \ddots & \vdots \\ L_{N2}(s) & \cdots & L_{NN}(s)\end{bmatrix}\begin{bmatrix}\Delta U_{\mathrm{dc2}} \\ \vdots \\ \Delta U_{\mathrm{dcN}}\end{bmatrix}\end{aligned} \tag{19}$$

The dynamics of the DC capacitors of VSCs except VSC 1 can be written as:

$$\begin{bmatrix}\Delta U_{\mathrm{dc2}} \\ \vdots \\ \Delta U_{\mathrm{dcN}}\end{bmatrix} = \begin{bmatrix}\frac{1}{sC_2U_{\mathrm{dc20}}} & & \\ & \ddots & \\ & & \frac{1}{sC_NU_{\mathrm{dcN0}}}\end{bmatrix}\begin{bmatrix}\Delta P_{\mathrm{dc2}} \\ \vdots \\ \Delta P_{\mathrm{dcN}}\end{bmatrix} \tag{20}$$

Invert (20) and substitute the result into (19).ΔUdc1 can represent the DC voltage of VSCs $2 \sim N_1$ as:

$$\begin{bmatrix}\Delta U_{\mathrm{dc2}} \\ \vdots \\ \Delta U_{\mathrm{dcN}}\end{bmatrix} = [\Phi_{ij}(s)]^{-1}\begin{bmatrix}L_{21} \\ \vdots \\ L_{N1}\end{bmatrix}\Delta U_{\mathrm{dc1}} \tag{21}$$

where

$$\Phi_{ij}(s)=\begin{cases} sC_iU_{\mathrm{dci0}}-L_{ii}(s), & i=j \\ -L_{ij}(s), & i\neq j \end{cases} \tag{22}$$

After that, substituting (21) into (18), the unbalanced active power can be computed as:

$$\begin{aligned}\Delta P_{\mathrm{dc1}}=&L_{11}(s)\Delta U_{\mathrm{dc1}}+\begin{bmatrix}L_{12}(s) & \cdots & L_{1N}(s)\end{bmatrix}\\ &\cdot\left\{[\Phi_{ij}(s)]^{-1}\begin{bmatrix}L_{21}(s)\\ \vdots\\ L_{N1}(s)\end{bmatrix}\right\}\Delta U_{\mathrm{dc1}}\end{aligned} \tag{23}$$

According to the definitions of SSC and ESC in (5), SSC equals to $L_{11}(s)$, and the overall ESC is

$$F_{\mathrm{E1}}(s)=\begin{bmatrix}L_{12}(s) & \cdots & L_{1N}(s)\end{bmatrix}\cdot\left\{[\Phi_{ij}(s)]^{-1}\begin{bmatrix}L_{21}(s)\\ \vdots\\ L_{N1}(s)\end{bmatrix}\right\} \tag{24}$$

Next, we can calculate the different terms of ESCs that reflect different paths of interaction.

3) Different Terms of ESCs

As mentioned in subsection A, to reflect different paths of interactions, the overall ESC can be decomposed into different terms according to the two principles. Based on *Principle* 1, i.e., the quantity of VSCs participating in the interactions, the ESC can be decomposed into single ESC, double ESC, triple ESC and so on. Based on *Principle* 2, i.e., different effects of DC and AC networks, the above items can be decomposed into one coupled only by the DC network and the other one coupled by both AC and DC networks. Different paths of ESCs are computed as follows.

Step 1: Decomposition of the ESC based on Principle 1. Considering the N-terminal HVDC system, $F_{\mathrm{E1}}(s)$ has $N-1$ types according to the quantity of VSCs participating in the interactions. For the interactions between VSC 1 and i, a single ESC can be written as:

$$F_{\mathrm{E1}}^{i}(s)=\frac{L_{i1}(s)L_{1i}(s)}{sC_iU_{\mathrm{dci0}}-L_{ii}(s)} \tag{25}$$

For the interactions among VSC i, j and VSC 1, double ESC can be calculated as:

$$\begin{aligned}F_{\mathrm{E1}}^{ij}(s)=&\begin{bmatrix}L_{1i}(s) & L_{1j}(s)\end{bmatrix}\\ &\cdot\left\{\begin{bmatrix}\Phi_{ii}(s) & \Phi_{ij}(s)\\ \Phi_{ji}(s) & \Phi_{jj}(s)\end{bmatrix}\right\}^{-1}\begin{bmatrix}L_{i1}(s)\\ L_{j1}(s)\end{bmatrix}\\ &-F_{\mathrm{E1}}^{i}(s)-F_{\mathrm{E1}}^{j}(s)\end{aligned} \tag{26}$$

For the interactions involving the most VSCs, the ESC among VSCs $2\sim N$ and VSC 1 can be expressed as:

$$\begin{aligned}F_{\mathrm{E1}}^{U}(s)=&F_{\mathrm{E1}}(s)\\ &-\left(\sum_{i=2}^{N}F_{\mathrm{E1}}^{i}(s)+\sum_{i=2,j=3,i<j}^{N}F_{\mathrm{E1}}^{ij}(s)+\cdots\right.\\ &\left.+\sum_{l=2}^{N-1}F_{\mathrm{E1}}^{J_l}(s)\right)\end{aligned} \tag{27}$$

where $U=\{2,3,\cdots,N\}, J_lU, J_lR^{1\times(N-2)}$, $l\in\{1,2,\cdots,N-1\}$. The rest of the terms can be calculated in the same manner.

Step 2: Decomposition of the en-stabilizing coefficient based on Principle 2. According to the different effects of DC and AC networks, ESCs can be subdivided into two terms. One is the interactions coupled only by the DC network, and the other is the interactions coupled by both DC and AC networks. From the results in (17), it is obvious that the first term of $\boldsymbol{L}(s)$, i.e., matrix $\boldsymbol{A}$, reflects the interactions coupled only by the DC network. Hence, ESCs coupled only by the DC network can be computed by

$$F_{\mathrm{E1}}^{iA}(s)=\frac{L_{1i}(s)A_{i1}}{sC_iU_{\mathrm{dci0}}-A_{ii}} \tag{28}$$

$$\begin{aligned}F_{\mathrm{E1}}^{ijA}(s)=&\begin{bmatrix}L_{1i}(s) & L_{1j}(s)\end{bmatrix}\\ &\cdot\left\{\begin{bmatrix}\Phi_{ii}(s) & \Phi_{ij}(s)\\ \Phi_{ji}(s) & \Phi_{jj}(s)\end{bmatrix}\right\}^{-1}\begin{bmatrix}A_{i1}\\ A_{j1}\end{bmatrix}\\ &-F_{\mathrm{E1}}^{iA}(s)-F_{\mathrm{E1}}^{jA}(s),\\ &\vdots\end{aligned} \tag{29}$$

$$\begin{aligned}F_{\mathrm{E1}}^{\mathrm{UA}}(s)=&\begin{bmatrix}L_{12}(s) & \cdots & L_{1N}(s)\end{bmatrix}\left\{[\Psi_{ij}(s)]^{-1}\begin{bmatrix}A_{21}\\ \vdots\\ A_{N1}\end{bmatrix}\right\}\\ &-\left(\sum_{i=2}^{N}F_{\mathrm{E1}}^{iA}(s)+\sum_{i=2,j=3,i<j}^{N}F_{\mathrm{E1}}^{ijA}(s)+\cdots\right.\\ &\left.+\sum_{l=2}^{N-1}F_{\mathrm{E1}}^{J_lA}(s)\right)\end{aligned} \tag{30}$$

where

$$\Psi_{ij}(s)=\begin{cases} sC_iU_{\mathrm{dci0}}-A_{ii}, & i=j \\ -A_{ij}, & i\neq j \end{cases} \tag{31}$$

Then, ESCs coupled by both DC and AC networks can be expressed as:

$$F_{\mathrm{E1}}^{iB}(s)=F_{\mathrm{E1}}^{i}(s)-F_{\mathrm{E1}}^{iA}(s) \tag{32}$$

$$F_{\mathrm{E1}}^{ijB}(s)=F_{\mathrm{E1}}^{ij}(s)-F_{\mathrm{E1}}^{ijA}(s) \tag{33}$$

$$F_{\mathrm{E1}}^{\mathrm{UB}}(s)=F_{\mathrm{E1}}^{U}(s)-F_{\mathrm{E1}}^{\mathrm{UA}}(s) \tag{34}$$

The small-signal model with quantification of the interactions can be depicted in Fig. 3(b).

Thus, different paths of interactions among the VSCs for the general N-terminal HVDC systems can be quantified by explicit formulae of self-/en-stabilizing coefficients. These formulae hold for any N and can be easily computed in current practical applications, of which N is less than 10. At the same time, it is still difficult to compute the transfer functions of large-scale MIMO systems with hundreds and thousands of equipment. The orders of such systems are so high that even if the transfer functions of the systems are derived, it is difficult to solve them numerically. This is the common challenge of all the analytical methods for stability analysis, including eigenvalue analysis, impedance analysis, and the net

damping method. These methods are usually used in small-scale systems to explore the mechanism and regularity of the stability.

In the next section, we will discuss the relationship between the interactions, parameters, and system stability.

IV. Stability Criterion and Parameter Sensitivity

In this section, we will present the stability criterion and parameter sensitivity of the proposed method. Firstly, the relation between the self-/en-stabilizing coefficients and the poles of the system is demonstrated to obtain the stability criterion. Secondly, we propose parameter sensitivity to analyze how the parameters affect the stability of the system through different paths of interactions.

A. Stability Criterion of the Method

Now we propose the stability criterion by demonstrating the relation between the self-/en-stabilizing coefficients and the poles of the system.

According to Fig. 3(b), the closed-loop transfer function of the system can be written as:

$$G(s)=\frac{1}{G_{\rm den}(s)}=\frac{1}{sC_iU_{\rm dci0}-(F_{Si}(s)+F_{Ei}(s))} \tag{35}$$

Obviously, the poles of the system can be computed by $G_{\rm den}(s)=0$. Assume that the conjugated poles closest to the imaginary axis in the DVC timescale are $\lambda_{i,j}=\sigma_0\pm j\omega_{\rm d}$. $G_{\rm den}(j\omega)$ can be expressed as:

$$G_{\rm den}(j\omega)=(j\omega-\lambda_i)(j\omega+\lambda_j)G_{\rm rest}(j\omega) \tag{36}$$

where $G_{\rm rest}(j\omega)$ represents the rest part of $G_{\rm den}(j\omega)$. $G_{\rm rest}(j\omega)=\alpha+j\beta$ at the oscillation frequency.

Then, the real part and imaginary part of the $G_{\rm den}(j\omega)$ can be calculated as:

$$\begin{aligned}\mathrm{Re}[G_{\rm den}(j\omega)]&=-\{\mathrm{Re}[F_{Si}(j\omega)]+\mathrm{Re}[F_{Ei}(j\omega)]\}\\&=\alpha(-\omega^2+\sigma_0^2+\omega_{\rm d}^2)+2\beta\sigma_0\omega,\end{aligned} \tag{37}$$

$$\mathrm{Im}[G_{\rm den}(j\omega)]=\beta(-\omega^2+\sigma_0^2+\omega_{\rm d}^2)-2\alpha\sigma_0\omega \tag{38}$$

Let $\mathrm{Im}[G_{\rm den}(j\omega)]=0$. The oscillation frequency can be computed as:

$$\omega_{s1,2}=-\frac{\alpha\sigma_0\pm\sqrt{\alpha^2\sigma_0^2+\beta^2(\sigma_0^2+\omega_{\rm d}^2)}}{\beta} \tag{39}$$

For a weak damping system, it has $\sigma_0\ll\omega_{\rm d}$, so $\omega_s\approx\omega_{\rm d}$.

Therefore, the relationship between the real part of the self-/en-stabilizing coefficients and the conjugated poles $\lambda_{i,j}$ can be written as:

$$\mathrm{Re}[F_{Si}(\mathrm{j}\omega)]+\mathrm{Re}[F_{Ei}(\mathrm{j}\omega)]\approx-2\beta\sigma_0\omega_{\rm d} \tag{40}$$

Since $\omega_{\rm d}>0$, we can evaluate the stability of the system based on the sign of β and $\mathrm{Re}[F_{Si}(\mathrm{j}\omega)]+\mathrm{Re}[F_{Ei}(\mathrm{j}\omega)]$.

According to (38), we can see that β determines the direction of $\mathrm{Im}[G_{\rm den}(\mathrm{j}\omega)]$ crossing the real axis. If $\beta>0$, $\mathrm{Im}[G_{\rm den}(\mathrm{j}\omega)]$ crosses the zero point from positive to negative. Otherwise, $\mathrm{Im}[G_{\rm den}(\mathrm{j}\omega)]$ crosses the zero point from negative to positive. Then the stability criterion can be described as follows.

- For $\beta>0$, if $\mathrm{Re}[F_{Si}(\mathrm{j}\omega)]+\mathrm{Re}[F_{Ei}(\mathrm{j}\omega)]>0$, then $\sigma_0<0$. It means when $\mathrm{Im}[G_{\rm den}(\mathrm{j}\omega)]$ crosses the zero point from positive to negative, if the real part of the sum of SSC and ESC are positive, the system is stable with negative poles. Otherwise, the system is unstable.
- For $\beta<0$, if $\mathrm{Re}[F_{Si}(\mathrm{j}\omega)]+\mathrm{Re}[F_{Ei}(\mathrm{j}\omega)]<0$, then $\sigma_0<0$. It means when $\mathrm{Im}[G_{\rm den}(\mathrm{j}\omega)]$ crosses the zero point from negative to positive, if the real part of the sum of SSC and ESC is negative, the system is stable with negative poles. Otherwise, the system is unstable.

Based on this stability criterion, we can evaluate the different effects of the interactions on the stability and explain which paths of the interactions cause the oscillation. Once the interactions of a certain system are analyzed using this method, one can even evaluate the stability of a system with reduced VSCs by existing results.

B. Parameter Sensitivity of the SSC and ESC

In order to analyze how different parameters influence different paths of interactions and further affect the system stability quantitatively, we propose the parameter sensitivity of this method.

Denote the variation of a controller or operation parameter as Δk. Denote the small variation of the real part of SSC and ESCs at $\omega=\omega_{\rm d}$ as $\Delta\mathrm{Re}[F_H(\mathrm{j}\omega)]$, where $F_H(\mathrm{j}\omega)$ represents any path of the SSC and ESCs. Set $k=k_0$ at the initial point. Then, we define the parameter sensitivity of the SSC and ESCs as:

$$Sen(k)=\lim_{\Delta k\to0}\frac{\Delta\mathrm{Re}[F_H(\mathrm{j}\omega)]}{\Delta k}=\left.\frac{\partial\mathrm{Re}[F_H(\mathrm{j}\omega)]}{\partial k}\right|_{\substack{\omega=\omega_{\rm d}\\k=k_0}} \tag{41}$$

By traversing different terms of SSC and ESCs for a concerned parameter, we can see the effects of this parameter on the stability through different paths. To be specific, the larger the absolute value of $Sen(k)$, the greater this parameter affects the stability through this path. Moreover, combined with the stability criterion in subsection A, we have the following inference: (i) For $\beta>0$, if $Sen(k)>0$, the system is more stable as k increases. Otherwise, the system is more unstable. (ii) For $\beta<0$, if $Sen(k)<0$, the system is more stable as k increases. Otherwise, the system is more unstable.

Case studies to analyze the interactions and the effect of the parameters on the system stability are presented in the next section.

V. Case Study

In this section, we will present several examples to show the effectiveness of the proposed method. First, we compare the proposed method with the modal analysis method and analyze how the interactions affect the system's stability. Then, we analyze the effect of PLL and short current ratio (SCR) on the stability through different paths of interactions. A four-terminal HVDC system shown in Fig. 4 is considered. Each VSC is connected with a weak AC grid, consisting of an equivalent reactance and an ideal voltage source. The voltage sources are considered without dynamics because the dynamics of one-mass SGs are in electromechanical timescale

(around 1 Hz), being much slower than the dynamics of VSCs in DVC timescale. System parameters and common control parameters are shown in Appendix B. Other specific parameters will be given in each case.

A. Interaction Analysis and Comparison with Modal Analysis

In the existing body of knowledge, modal analysis is one of the most common methods for interaction analysis. In this subsection, we will compare with modal analysis to show the connotations of interactions obtained by the proposed method.

Consider the system in Fig. 4 with the given parameters in Appendix B. Set $k_{32} = 5$, $k_{42} = 2000$, $X_{g3} = 0.2$, $P_{30} = 0.8$. Table I lists the results of eigenvalues (except for the real roots) and participation factors in the DVC timescale. We can see that DC voltage control and PLL of VSC 2 dominate $\lambda_{1,2}$. However, the results could not solve the following problems that we are interested in: (i) Which kind of interactions caused the oscillation? (ii) How did the control parameters influence the system stability through different paths of interactions? We will use our proposed method to solve the first problem in this subsection and solve the second problem in the next subsection.

Now we present two cases to analyze which paths of the interactions cause the oscillation.

TABLE I
RESULTS OF MODEL ANALYSIS IN DVC TIMESCALE

λ in the DVC timescale		States with participation factors >0.05
$\lambda_{1,2}$	2.11±j53.13	ΔU_{dc2}, Δi_{d2}, $\Delta\theta_{p2}$, $\Delta\omega_{p2}$
$\lambda_{3,4}$	−4.46±j99.69	ΔI_{dc1}, ΔI_{dc2}, ΔI_{dc4}, ΔU_{dc1}, ΔU_{dc2}, ΔU_{dc4}, $\Delta\theta_{p4}$, Δi_{d4}
$\lambda_{5,6}$	−9.32±j204.71	ΔI_{dc1}, ΔI_{dc2}, ΔI_{dc4}, ΔU_{dc3}, Δi_{d3}
$\lambda_{7,8}$	−16.47±j94.69	ΔI_{dc1}, ΔI_{dc2}, ΔU_{dc1}, ΔU_{dc2}, ΔU_{dc4}, $\Delta\theta_{p1}$, Δi_{d1}, Δi_{d4}
$\lambda_{9,10}$	−20.97±j50.67	ΔU_{dc1}, ΔU_{dc2}, $\Delta\theta_{p1}$, Δi_{d1}, $\Delta\omega_{p1}$, $\Delta\theta_{p4}$, $\Delta\omega_{p4}$, $\Delta\theta_{p2}$, Δi_{d2}, $\Delta\omega_{p2}$
$\lambda_{11,12}$	−26.74±j37.65	$\Delta\theta_{p1}$, $\Delta\omega_{p1}$, $\Delta\theta_{p3}$, $\Delta\omega_{p3}$,
$\lambda_{13,14}$	−31.44±j33.36	ΔU_{dc3}, ΔU_{dc1}, $\Delta\theta_{p1}$, Δi_{d1}, $\Delta\omega_{p1}$, $\Delta\theta_{p4}$, Δi_{d4}, $\Delta\omega_{p4}$, $\Delta\theta_{p3}$, Δi_{d3}, $\Delta\omega_{p3}$
$\lambda_{15,16}$	−34.66±j38.84	ΔI_{dc4}, ΔU_{dc1}, $\Delta\theta_{p1}$, Δi_{d1}, $\Delta\omega_{p1}$, $\Delta\theta_{p4}$, Δi_{d4}, $\Delta\omega_{p4}$

Case 1: Consider the system with the same parameters as modal analysis. When focusing on VSC 1, Fig. 5(a) shows the frequency characteristics of the real part of SSC and ESCs through different paths. Note that in most cases (including the cases in this paper), $\mathrm{Im}[G_{\mathrm{den}}(\mathrm{j}\omega)]$ crosses the zero point from negative to positive, i.e. β <0. The oscillation frequency is $\omega_{d1} = 53.1$ rad/s. In Fig. 5(a), $\mathrm{Re}[F_{\mathrm{E1}}^{3\mathrm{A}}(s)]$ and $\mathrm{Re}[F_{\mathrm{E1}}^{34\mathrm{B}}(s)]$ has the largest two negative values to make the system stable, while $\mathrm{Re}[F_{\mathrm{S1}}(s)]$ and $\mathrm{Re}[F_{\mathrm{E1}}^{234\mathrm{B}}(s)]$ have the largest two positive values to make the system unstable. Since

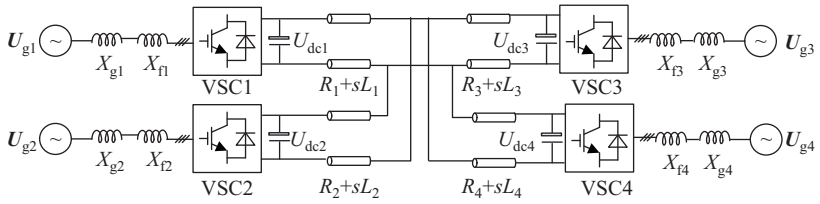

Fig. 4. A four-terminal HVDC system connected with weak AC grids.

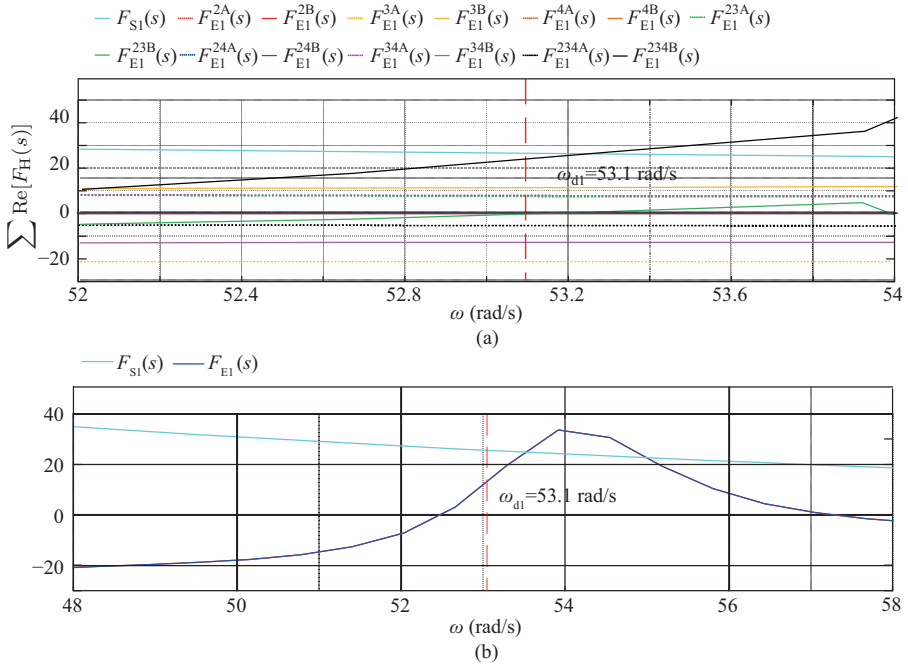

Fig. 5. Frequency characteristics of the real part of the SSC and ESCs through different paths in Case 1. (a) Frequency characteristics of SSC and different paths of ESCs in Case 1. (b) Frequency characteristics of SSC and overall ESC in Case 1.

$\mathrm{Re}[F_{\mathrm{E1}}(\mathrm{j}\omega)+F_{\mathrm{S1}}(\mathrm{j}\omega)]>0$ as shown by Fig. 5(b), the system is unstable. The results indicate that $\mathrm{Re}[F_{\mathrm{E1}}^{234\mathrm{B}}(s)]$ dominates the instability of the system. Hence, we should pay more attention on $\mathrm{Re}[F_{\mathrm{E1}}^{234\mathrm{B}}(s)]$.

Moreover, in Fig. 5(a), we can see that $F_{\mathrm{E1}}^{2\mathrm{A}}(s)=F_{\mathrm{E1}}^{2\mathrm{B}}(s)=F_{\mathrm{E1}}^{4\mathrm{A}}(s)=F_{\mathrm{E1}}^{4\mathrm{B}}(s)=0$, which means that VSC 2 and 4 do not interact with VSC 1 directly. This phenomenon can be explained as follows. As the same as Cigre B4 HVDC benchmark [2], the point of common coupling in the DC network in Fig. 4 is close to the inverter, i.e., VSC 3. Therefore, $R_3=L_3=0$ p.u.. The admittance matrix of the DC network $[y_{ij}]$ and matrix $\boldsymbol{A}$ reflecting the power flow in the DC network can be calculated according to the system parameters. The results are shown in Appendix C, where $A_{12}=A_{14}=A_{21}=A_{41}=0$. So we have $\Delta P_{\mathrm{in}1}=A_{11}\Delta U_{\mathrm{dc}1}+A_{13}\Delta U_{\mathrm{dc}3}$. It means that $\Delta P_{\mathrm{in}1}$ does not respond to the variation of $\Delta U_{\mathrm{dc}2}$ and $\Delta U_{\mathrm{dc}4}$ directly. When $\Delta U_{\mathrm{dc}2}$ or $\Delta U_{\mathrm{dc}4}$ varies, $\Delta U_{\mathrm{dc}3}$ and $\Delta P_{\mathrm{in}3}$ vary first. Then, $\Delta P_{\mathrm{in}1}$ and $\Delta U_{\mathrm{dc}1}$ change with the variation of $\Delta U_{\mathrm{dc}3}$.

We perform the following experiments to prove the correctness of the analysis results further. When VSC 1 connects to an ideal DC source, the oscillation frequency can be calculated by $\mathrm{Im}[G_{\mathrm{den}}(\mathrm{j}\omega)]=0$. The system is stable on this occasion because $\mathrm{Re}[F_{\mathrm{S1}}(s)]<0$ at $\omega_{\mathrm{S}}=98.54$ rad/s. Then, based on the results in Fig. 5(a), when VSC 1 is connected to VSC 2, the dynamic performance of VSC 1 would not change because $F_{\mathrm{E1}}^{2\mathrm{A}}(s)=F_{\mathrm{E1}}^{2B}(s)=0$. When VSC 1 connects to VSC 2 and 3, the oscillation frequency is about 53.5 rad/s. Since $\mathrm{Re}[F_{\mathrm{E1}}^{3\mathrm{A}}(s)+F_{\mathrm{E1}}^{3\mathrm{B}}(s)+F_{\mathrm{E1}}^{23\mathrm{A}}(s)+F_{\mathrm{E1}}^{23\mathrm{B}}(s)]\approx-3$ and $\mathrm{Re}[F_{\mathrm{S1}}(s)]\approx25$, the system would be unstable. When VSC 1 connects to VSC 2∼4, we have $\mathrm{Re}[F_{\mathrm{E1}}^{234\mathrm{A}}(s)+F_{\mathrm{E1}}^{234\mathrm{B}}(s)]\approx9>0$ and $F_{\mathrm{E1}}^{4\mathrm{A}}(s)=F_{\mathrm{E1}}^{4\mathrm{B}}(s)=F_{\mathrm{E1}}^{24\mathrm{A}}(s)=F_{\mathrm{E1}}^{24\mathrm{B}}(s)=0$ at $\omega_{\mathrm{d}1}=53.1$ rad/s. This means that the oscillation will be more severe due to the positive value of $\mathrm{Re}[F_{\mathrm{E1}}^{234\mathrm{A}}(s)+F_{\mathrm{E1}}^{234\mathrm{B}}(s)]$. Time domain simulation obtained from a non-linear detailed model verifies the results as shown by Fig. 6.

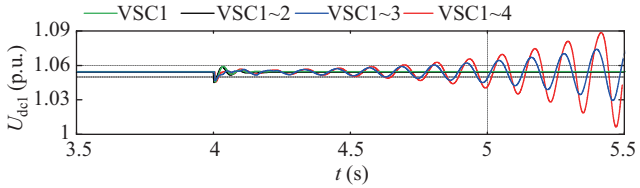

Fig. 6. Time domain responses of DC voltage of VSC 1 connected to different quantities of VSCs.

Case 2: Consider the system in Fig. 4 with $k_{32}=10$, $k_{42}=2000$, $X_{\mathrm{g}3}=0.8$, $P_{30}=0.8$. Fig. 7(a) shows the frequency characteristics of the real part of SSC and ESCs through different paths. At $\omega_{\mathrm{d}2}=62.7$ rad/s, we can see that $\mathrm{Re}[F_{\mathrm{E1}}^{3\mathrm{A}}(s)]$, $\mathrm{Re}[F_{\mathrm{E1}}^{23\mathrm{B}}(s)]$ and $\mathrm{Re}[F_{\mathrm{E1}}^{34\mathrm{B}}(s)]$ are negative to make the system stable, while $\mathrm{Re}[F_{\mathrm{S1}}(s)]$ and $\mathrm{Re}[F_{\mathrm{E1}}^{3\mathrm{B}}(s)]$ with the largest two positive value do harm to the stability of the system. The system is unstable since $\mathrm{Re}[F_{\mathrm{E1}}(\mathrm{j}\omega)+F_{\mathrm{S1}}(\mathrm{j}\omega)]>0$ as shown by Fig. 7(b). Hence, we should pay more attention on $\mathrm{Re}[F_{\mathrm{E1}}^{3\mathrm{B}}(s)]$, which dominates the instability of the system.

The correctness of the results in Fig. 7(a) can also be proved. As in Case 1, VSC 1 is stable when it connects to an ideal DC source. When it only connects to VSC 3, the system would be stable since $\mathrm{Re}[F_{\mathrm{S1}}(s)+F_{\mathrm{E1}}^{3\mathrm{A}}(s)+F_{\mathrm{E1}}^{3\mathrm{B}}(s)]<0$ at the calculated oscillation frequency $\omega_{\mathrm{S}}=58.8$ rad/s. When VSC 1 connects to VSC 3 and 4, the system remains stable because $\mathrm{Re}[F_{\mathrm{S1}}(s)+F_{\mathrm{E1}}^{3\mathrm{A}}(s)+F_{\mathrm{E1}}^{3\mathrm{B}}(s)+F_{\mathrm{E1}}^{34\mathrm{A}}(s)+F_{\mathrm{E1}}^{34\mathrm{B}}(s)]<0$ and $\mathrm{Re}[F_{\mathrm{E1}}^{4\mathrm{A}}(s)+F_{\mathrm{E1}}^{4\mathrm{B}}(s)]=0$ at $\omega_{\mathrm{S}}=68.5$ rad/s. When

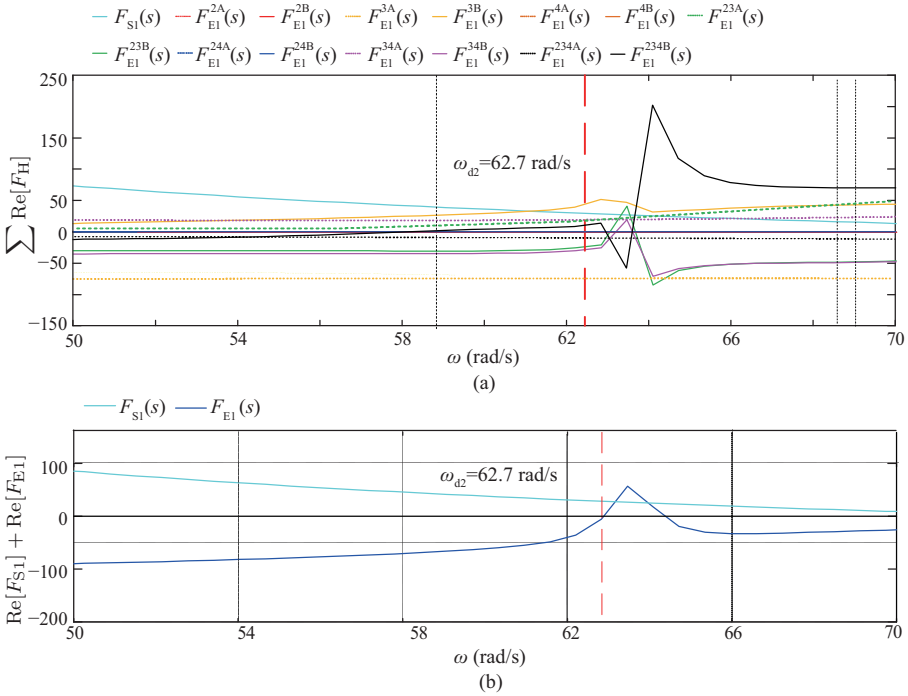

Fig. 7. Frequency characteristics of the real part of SSC and ESCs through different paths in Case 2. (a) Frequency characteristics of SSC and different paths of ESCs in Case 2. (b) Frequency characteristics of SSC and overall ESC in Case 2.

VSC 1 connects to VSC 2 and 3, the oscillation frequency is 69.0 rad/s. Since $\mathrm{Re}[F_{\mathrm{E1}}^{23\mathrm{A}}(s)+F_{\mathrm{E1}}^{23\mathrm{B}}(s)]$ at 69.0 rad/s is larger than $\mathrm{Re}[F_{\mathrm{E1}}^{34\mathrm{A}}(s)+F_{\mathrm{E1}}^{34\mathrm{B}}(s)]$ at 68.5 rad/s, the stability of VSC 1 connected with VSC 2 and 3 would be worse than the stability of VSC 1 connected with VSC 3 and 4. Moreover, when VSC 1 connects with VSC 2∼4, the system has the worst stability performance because $\mathrm{Re}[F_{\mathrm{S1}}(s)+F_{\mathrm{E1}}(s)]$ at $\omega_{\mathrm{d2}}=62.7$ rad/s is positive with the largest value among the above situations. The time domain simulation in Fig. 8 verifies the results.

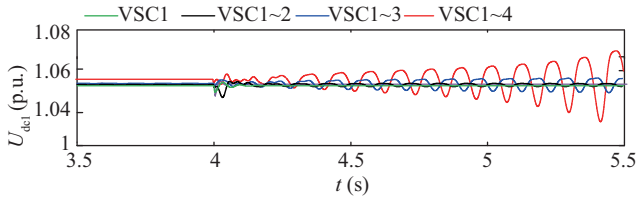

Fig. 8. Time domain responses of DC voltage of VSC 1 connected to different quantities of VSCs.

B. Effect of Parameters of PLL and SCR.

In this subsection, we will analyze how the parameters of PLL and the SCR affect the system stability through different paths of interactions.

First, let us analyze the effect of the parameters of PLL in VSC 2. Set $X_{\mathrm{g3}}=0.2$, $P_{30}=0.8$. Note that k_{32} and k_{42} appear in the paths related to VSC 2. Set $k_{32}=10$, $k_{42}=2000$ as the initial point. Table II lists the sensitivity of different paths of ESCs with respect to k_{32} and k_{42}. The results show that $\mathrm{Re}[F_{\mathrm{E1}}^{23\mathrm{B}}(s)]$ and $\mathrm{Re}[F_{\mathrm{E1}}^{234\mathrm{B}}(s)]$ are sensitive to the variation of k_{32} and k_{42}. Moreover, since $\beta<0$ and $\mathrm{Re}[F_{\mathrm{E1}}^{23\mathrm{B}}(s)]$ and $\mathrm{Re}[F_{\mathrm{E1}}^{234\mathrm{B}}(s)]$ decreases with the increase of k_{32}, the system becomes more stable as k_{32} increases. Since $\mathrm{Re}[F_{\mathrm{E1}}^{23\mathrm{B}}(s)]$ and $\mathrm{Re}[F_{\mathrm{E1}}^{234\mathrm{B}}(s)]$ increase with the increase of k_{42}, the system is more stable as k_{42} decreases. The results can be verified by time domain simulation as depicted in Figs. 9 and 10. Therefore, we should pay much attention to $\mathrm{Re}[F_{\mathrm{E1}}^{23\mathrm{B}}(s)]$ and $\mathrm{Re}[F_{\mathrm{E1}}^{234\mathrm{B}}(s)]$ when we set or tune the parameters of PLL in VSC 2.

Next, we analyze how the SCR of AC grid 3 affects the stability of the system. Set $k_{32}=10$, $k_{42}=2000$. Note that SCR is determined by X_{g3} and P_{30}, which appear in all the paths related to VSC 3. Set $X_{\mathrm{g3}}=0.4$, $P_{30}=0.8$ as the initial point. Table III lists the sensitivity of different paths

TABLE II
THE SENSITIVITY OF DIFFERENT PATHS OF ESCS WITH RESPECT TO THE PARAMETERS OF PLL

Description	$F_{\mathrm{E1}}^{2\mathrm{B}}(s)$	$F_{\mathrm{E1}}^{23\mathrm{B}}(s)$	$F_{\mathrm{E1}}^{24\mathrm{B}}(s)$	$F_{\mathrm{E1}}^{234\mathrm{B}}(s)$
$Sen(k_{32})$	0	−0.3113	0	−0.4842
$Sen(k_{42})$	0	0.0075	0	0.0193

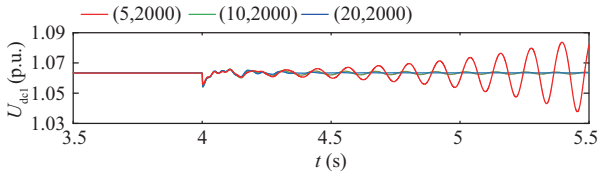

Fig. 9. Time domain responses of DC voltage of VSC 1 with different k_{32} of PLL in VSC 2.

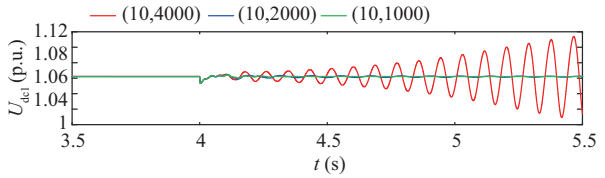

Fig. 10. Time domain responses of DC voltage of VSC 1 with different control parameters of PLL (k_{42}) of VSC 2.

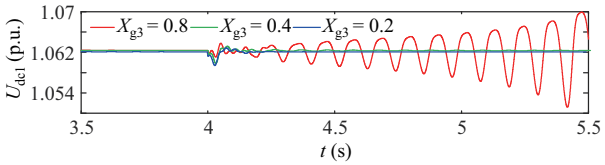

Fig. 11. Time domain responses of DC voltage of VSC 1 with different transmission line reactance of VSC 3.

of ESCs with respect to X_{g3} and P_{30}. For X_{g3}, the results show that all the paths are sensitive to it. All the real part of the interaction paths except for $F_{\mathrm{E1}}^{234\mathrm{B}}(s)$ increases with the increase of X_{g3}. This illustrates that different paths of interactions may have opposite effects on the stability with the variation of parameters. Since $Sen(P_{30})$ with respect to $\mathrm{Re}[F_{\mathrm{E1}}(s)]$ is positive, the system becomes more unstable with larger X_{g3}. The time domain simulation in Fig. 11 verifies the analysis. For P_{30}, $\mathrm{Re}[F_{\mathrm{E1}}^{3\mathrm{B}}(s)]$ and $\mathrm{Re}[F_{\mathrm{E1}}^{234\mathrm{B}}(s)]$ are more sensitive to it, and they have an opposite influence on the stability with the variation of P_{30}. At the same time, the whole system is more stable with a smaller P_{30}. The time domain simulation in Fig. 12 verifies the results.

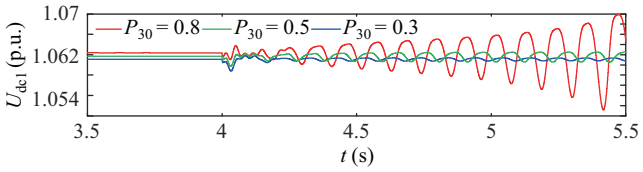

Fig. 12. Time domain responses of DC voltage of VSC 1 with different active power of VSC 3.

The analysis above shows the effectiveness of the method in revealing insights about the interactions. It also provides a new idea for the setting and tuning of a control parameter.

TABLE III
THE SENSITIVITY OF DIFFERENT PATHS OF ESCS WITH RESPECT TO SCR

Description	$\mathrm{Re}[F_{\mathrm{E1}}^{3\mathrm{B}}(s)]$	$\mathrm{Re}[F_{\mathrm{E1}}^{23\mathrm{B}}(s)]$	$\mathrm{Re}[F_{\mathrm{E1}}^{34\mathrm{B}}(s)]$	$\mathrm{Re}[F_{\mathrm{E1}}^{234\mathrm{B}}(s)]$	$\mathrm{Re}[F_{\mathrm{E1}}(s)]$
$Sen(X_{\mathrm{g3}})\omega_{\mathrm{d2}}=62.7$	15.48	30.65	24.02	−34.07	36.09
$Sen(P_{30})\omega_{\mathrm{d3}}=71.9$	−8.23	1.32	3.98	15.01	0.30

That is, if part of the system changes, it may be possible only to consider the part of the system related to the concerned parameters rather than the overall system. We will investigate this further in the future.

VI. Conclusion

This paper has proposed a method to quantify the interactions among VSCs of the N-terminal HVDC system connected with weak AC grids. We have derived explicit formulae of the self-/en-stabilizing coefficients of the N-terminal HVDC system, which can quantify the interactions through different paths analytically. Then, we presented the stability criterion of this method by demonstrating the relation between the self-/en-stabilizing coefficients and the poles of the system. Based on the criterion, we can evaluate the impact of the interactions on the stability of the system through different paths. Moreover, the parameter sensitivity of this method is proposed. It can help quantify the influence of different parameters on the system stability through different paths of interactions. We have given several simulation examples to show the advantages and effectiveness of our proposed method.

This method can reveal more insights into the linear process of the interactions among VSCs and provide new ideas for the setting and tuning of control parameters in MTDC systems. In future research, it is worthwhile to propose the MMC model for the interaction analysis, analyze the interactions among controllers of a single VSC in multiple timescales, and study the interaction dynamics directly based on a general nonlinear model.

Appendix

A. Specific Expressions of Transfer Functions.

$$\varepsilon_{0i} = \frac{X_{\mathrm{fi}} C_i U_{\mathrm{dci0}}}{E_{i0}(E_{i0} - U_{\mathrm{ti0}})}$$

$$\varepsilon_{1i} = \frac{C_i U_{\mathrm{dci0}} X_{\mathrm{fi}} k_{3i}}{E_{i0} - U_{\mathrm{ti0}}} + \frac{(U_{\mathrm{dci0}}^2 + k_{\mathrm{di}} P_{i0}) X_{\mathrm{fi}} k_{1i}}{U_{\mathrm{dci0}}^2 (E_{i0} - U_{\mathrm{ti0}})}$$

$$\varepsilon_{2i} = \frac{C_i U_{\mathrm{dci0}} X_{\mathrm{fi}} k_{4i}}{E_{i0} - U_{\mathrm{ti0}}} + \frac{(U_{\mathrm{dci0}}^2 + k_{\mathrm{di}} P_{i0})(X_{\mathrm{fi}} U_{\mathrm{ti0}} k_{1i} k_{3i} + X_{\mathrm{fi}} k_{2i})}{U_{\mathrm{dci0}}^2 (E_{i0} - U_{\mathrm{ti0}})}$$

$$\varepsilon_{3i} = \frac{X_{\mathrm{f}i} U_{\mathrm{t}i0} (U_{\mathrm{dci0}}^2 + k_{\mathrm{di}} P_{i0})(k_{1i} k_{4i} + k_{2i} k_{3i})}{U_{\mathrm{dci0}}^2 (E_{i0} - U_{\mathrm{t}i0})}$$

$$\varepsilon_{4i} = \frac{(U_{\mathrm{dci0}}^2 + k_{\mathrm{di}} P_{i0}) X_{\mathrm{f}i} U_{\mathrm{t}i0} k_{2i} k_{4i}}{U_{\mathrm{dci0}}^2 (E_{i0} - U_{\mathrm{t}i0})}$$

$$G_{\mathrm{ini}}(s) = \frac{X_{\mathrm{fi}} s^2 + X_{\mathrm{fi}} E_{i0} k_{3i} s + X_{\mathrm{fi}} E_{i0} k_{4i}}{(E_{i0} - U_{\mathrm{ti0}}) E_{i0} s^2} + \frac{k_{\mathrm{di}} X_{\mathrm{fi}} (k_{1i} s + k_{2i})(s^2 + U_{\mathrm{ti0}} k_{3i} s + U_{\mathrm{ti0}} k_{4i})}{U_{\mathrm{dci0}} (E_{i0} - U_{\mathrm{ti0}}) s^3}$$

$$G_{\mathrm{qi}}(s) = \frac{E_{i0}^2 X_{\mathrm{fi}} (s k_{5i} + s + k_{6i})}{(E_{i0} - U_{\mathrm{ti0}}) E_{i0} s}$$

B. System and Control Parameters

1) Steady-state Reference Values

Inspecting power $S_{\mathrm{base}} = 1000$ MVA. Peak phase voltage value $U_{\mathrm{base}} = 270$ kV. Frequency $f_{\mathrm{base}} = 50$ Hz. DC voltage $U_{\mathrm{dcbase}} = 400$ kV

2) Per-unit Values

VSC A $P_{10} = -0.4$ p.u., $Q_{10} = 0.5$ p.u., $U_{\mathrm{dc10}} = 1$ p.u., $U_{\mathrm{t10}} = 1$ p.u., $U_{\mathrm{g10}} = 1$ p.u., $C_1 = 0.05$ p.u., $X_{f1} = 0.25$ p.u., $X_{\mathrm{g1}} = 0.75$ p.u., $R_1 = 0.4$ p.u., $L_1 = 0.01$ p.u.

VSC B $P_{20} = -0.3$ p.u., $Q_{20} = 0.5$ p.u., $U_{\mathrm{dc20}} = 1$ p.u., $U_{\mathrm{t20}} = 1$ p.u., $U_{\mathrm{g20}} = 1$ p.u., $C_2 = 0.05$ p.u., $X_{f2} = 0.25$ p.u., $X_{\mathrm{g2}} = 1.25$ p.u., $R_2 = 0.4$ p.u., $L_2 = 0.01$ p.u.

VSC C $P_{30} = 0.8$ p.u., $Q_{30} = 0.5$ p.u., $U_{\mathrm{dc30}} = 1$ p.u., $U_{\mathrm{t30}} = 1$ p.u., $U_{\mathrm{g30}} = 1$ p.u., $C_3 = 0.05$ p.u., $X_{f3} = 0.25$ p.u., $R_3 = 0$ p.u., $L_3 = 0$ p.u.

VSC D $P_{40} = -0.1$ p.u., $Q_{40} = 0.5$ p.u., $U_{\mathrm{dc40}} = 1$ p.u., $U_{\mathrm{t40}} = 1$ p.u., $U_{\mathrm{g40}} = 1$ p.u., $C_4 = 0.05$ p.u., $X_{f4} = 0.25$ p.u., $X_{\mathrm{g4}} = 3.25$ p.u., $R_4 = 0.4$ p.u., $L_4 = 0.01$ p.u.

3) Common Control Parameters

DVC $k_{11} = 2.39$, $k_{12} = 1.5$, $k_{13} = k_{14} = 2$, $k_{21} = 113.7$, $k_{22} = k_{23} = k_{24} = 110$.

PLL control $k_{31} = k_{33} = k_{34} = 50$, $k_{41} = k_{43} = k_{44} = 2000$.

Droop control $k_{\mathrm{d1}} = k_{\mathrm{d2}} = k_{\mathrm{d4}} = 1.5$, $k_{\mathrm{d3}} = 2$.

ACC $k_{71} = k_{72} = k_{73} = k_8 = 0.6$, $k_{81} = k_{81} = k_{83} = k_{84} = 640$.

C. Specific Expressions of $[y_{ij}]$ and $\boldsymbol{A}$ in the Case Studies

$$[y_{ij}] = \begin{bmatrix} -\frac{1}{L_1 s + R_1} & 0 & \frac{1}{L_1 s + R_1} & 0 \\ 0 & -\frac{1}{L_2 s + R_2} & \frac{1}{L_2 s + R_2} & 0 \\ \frac{1}{L_1 s + R_1} & \frac{1}{L_2 s + R_2} & -\frac{1}{L_1 s + R_1} - \frac{1}{L_2 s + R_2} - \frac{1}{L_4 s + R_4} & \frac{1}{L_4 s + R_4} \\ 0 & 0 & \frac{1}{L_4 s + R_4} & -\frac{1}{L_4 s + R_4} \end{bmatrix}$$

$$\boldsymbol{A} = \begin{bmatrix} I_{\mathrm{dc10}} - \frac{U_{\mathrm{dc10}}}{L_1 s + R_1} & 0 & \frac{U_{\mathrm{dc10}}}{L_1 s + R_1} & 0 \\ 0 & I_{\mathrm{dc20}} - \frac{U_{\mathrm{dc20}}}{L_2 s + R_2} & \frac{U_{\mathrm{dc20}}}{L_2 s + R_2} & 0 \\ \frac{U_{\mathrm{dc30}}}{L_1 s + R_1} & \frac{U_{\mathrm{dc30}}}{L_2 s + R_2} & I_{\mathrm{dc30}} - \frac{U_{\mathrm{dc30}}}{L_1 s + R_1} - \frac{U_{\mathrm{dc30}}}{L_2 s + R_2} - \frac{U_{\mathrm{dc30}}}{L_4 s + R_4} & \frac{U_{\mathrm{dc30}}}{L_4 s + R_4} \\ 0 & 0 & \frac{U_{\mathrm{dc40}}}{L_4 s + R_4} & I_{\mathrm{dc40}} - \frac{U_{\mathrm{dc40}}}{L_4 s + R_4} \end{bmatrix}$$

References

[1] G. Asplund, K. Lindén, and C. Barker, "HVDC grid feasibility study," CIGRE, WG B4.52, 2013.

[2] "The CIGRE B4 DC grid test system," CIGRE, 2013.

[3] H. R. Wickramasinghe, G. Konstantinou, Z. X. Li, and J. Pou, "Alternate arm converters-based HVDC model compatible with the CIGRE B4 DC grid test system," *IEEE Transactions on Power Delivery*, vol. 34, no. 1, pp. 149–159, Feb. 2019.

[4] M. F. M. Arani and Y. A. R. I. Mohamed, "Analysis and performance enhancement of vector-controlled VSC in HVDC links connected to very weak grids," *IEEE Transactions on Power Systems*, vol. 32, no. 1, pp. 684–693, Jan. 2017.

[5] X. B. Zhao, J. Z. Xu, G. Li, J. S. Yuan and J. Liang, "Coordinated control of DC circuit breakers in multilink HVDC grids," *CSEE Journal of Power and Energy Systems*, vol. 9, no. 6, pp. 2224–2235, Nov. 2023.

[6] G. F. Tang, Z. Y. He, H. Pang, X. M. Huang, and X. P. Zhang, "Basic topology and key devices of the five-terminal DC grid," *CSEE Journal of Power and Energy Systems*, vol. 1, no. 2, pp. 22–35, Jun. 2015.

[7] G. O. Kalcon, G. P. Adam, O. Anaya-Lara, S. Lo, and K. Uhlen, "Small-signal stability analysis of multi-terminal VSC-based DC transmission systems," *IEEE Transactions on Power Systems*, vol. 27, no. 4, pp. 1818–1830, Nov. 2012.

[8] N. R. Chaudhuri, R. Majumder, B. Chaudhuri, and J. P. Pan, "Stability analysis of VSC MTDC grids connected to multimachine AC systems," *IEEE Transactions on Power Delivery*, vol. 26, no. 4, pp. 2774–2784, Oct. 2011.

[9] B. B. Shao, S. Q. Zhao, Y. H. Yang, B. F. Gao, and F. Blaabjerg, "Sub-synchronous oscillation characteristics and analysis of direct-drive wind farms with VSC-HVDC systems," *IEEE Transactions on Sustainable Energy*, vol. 12, no. 2, pp. 1127–1140, Apr. 2021.

[10] J. Sun and H. C. Liu, "Sequence impedance modeling of modular multilevel converters," *IEEE Journal of Emerging and Selected Topics in Power Electronics*, vol. 5, no. 4, pp. 1427–1443, Dec. 2017.
[11] J. Lyu, X. Zhang, X. Cai, and M. Molinas, "Harmonic state-space based small-signal impedance modeling of a modular multilevel converter with consideration of internal harmonic dynamics," *IEEE Transactions on Power Electronics*, vol. 34, no. 3, pp. 2134–2148, Mar. 2019.
[12] D. P. Lu, X. F. Wang, and F. Blaabjerg, "Impedance-based analysis of DC-link voltage dynamics in voltage-source converters," *IEEE Transactions on Power Electronics*, vol. 34, no. 4, pp. 3973–3985, Apr. 2019.
[13] L. Xu, L. L. Fan, and Z. X. Miao, "DC impedance-model-based resonance analysis of a VSC–HVDC system," *IEEE Transactions on Power Delivery*, vol. 30, no. 3, pp. 1221–1230, Jun. 2015.
[14] Y. Zhan, X. R. Xie, H. K. Liu, H. Liu, and Y. H. Li, "Frequency-domain modal analysis of the oscillatory stability of power systems with high-penetration renewables," *IEEE Transactions on Sustainable Energy*, vol. 10, no. 3, pp. 1534–1543, Jul. 2019.
[15] K. Ji, H. Pang, S. Liu and G. F. Tang, "Impedance analysis considering unstable subsystem poles for MMC-HVDC-based wind farm integration system," *CSEE Journal of Power and Energy Systems*, vol. 8, no. 2, pp. 634–639, Mar. 2022.
[16] P. Y. Wang, S. H. Feng, P. C. Liu, N. Q. Jiang and X.-P. Zhang, "Nyquist stability analysis and capacitance selection for DC current flow controllers in meshed multi-terminal HVDC grids," *CSEE Journal of Power and Energy Systems*, vol. 7, no. 1, pp. 114–127, Jan. 2021.
[17] Q. Fu, W. J. Du, H. F. Wang, and B. X. Ren, "Analysis of small-signal power oscillations in MTDC power transmission system," *IEEE Transactions on Power Systems*, vol. 36, no. 4, pp. 3248–3259, Jul. 2021.
[18] W. J. Du, Q. Fu, and H. F. Wang, "Small-signal stability of an AC/MTDC power system as affected by open-loop modal coupling between the VSCs," *IEEE Transactions on Power Systems*, vol. 33, no. 3, pp. 3143–3152, May 2018.
[19] Z. J. Zhen, W. J. Du, and H. F. Wang, "The proof of the equivalence of complex torque coefficient method and open-loop mode stabilization judgement method in strong mode coupling phenomena," *Proceedings of the CSEE*, vol. 39, no. 8, pp. 2272–2279, Apr. 2019.
[20] W. N. Zheng, J. B. Hu, and X. M. Yuan, "Analytic quantification of interactions in MTDC systems based on self-/en-stabilizing coefficients in DC voltage control timescale," *IEEE Journal of Emerging and Selected Topics in Power Electronics*, vol. 9, no. 3, pp. 2980–2991, Jun. 2021.
[21] J. W. He, B. Li, Y. Li, H. Qiu, C. Q. Wang, and D. K. Dai, "A fast directional pilot protection scheme for the MMC-based MTDC grid," *Proceedings of the CSEE*, vol. 37, no. 23, pp. 6878–6887, Dec. 2017.
[22] C. Y. Li, A. M. Gole, and C. Y. Zhao, "A fast DC fault detection method using DC reactor voltages in HVDC grids," *IEEE Transactions on Power Delivery*, vol. 33, no. 5, pp. 2254–2264, Oct. 2018.
[23] H. Yuan, X. M. Yuan, and J. B. Hu, "Modeling of grid-connected VSCs for power system small-signal stability analysis in DC-link voltage control timescale," *IEEE Transactions on Power Systems*, vol. 32, no. 5, pp. 3981–3991, Sep. 2017.
[24] W. N. Zheng, J. B. Hu, and X. M. Yuan, "Modeling of VSCs considering input and output active power dynamics for multi-terminal HVDC interaction analysis in DC Voltage Control Timescale," *IEEE Transactions on Energy Conversion*, vol. 34, no. 4, pp. 2008–2018, Dec. 2019.
[25] Ludvika, "Estlink HVDC light transmission system, 350MW±150kV, including 105km cables," ABB Power Tech. AB, SE., Feb. 2007.
[26] Ludvika, "Grid connection of offshore wind farms-Nord E. ON 1," ABB AB, SE., Pam. POW-0050, Nov. 2008.
[27] Ludvika, "Powering Valhall platform with HVDC Light," ABB AB, SE., Pam. POW-0049, Feb. 2009.
[28] J. B. Hu, J. H. Zhu, and M. Wan, "Modeling and analysis of modular multilevel converter in DC voltage control timescale," *IEEE Transactions on Industrial Electronics*, vol. 66, no. 8, pp. 6449–6459, Aug. 2019.

Wanning Zheng received the B.Eng. and Ph.D. degrees from the School of Electrical and Electronic Engineering, Huazhong University of Science and Technology, Wuhan, China, in July 2014 and July 2020, respectively. Now she is a Lecturer in Engineering Research Center of Metallurgical Automation and Measurement Technology, Wuhan University of Science and Technology, Wuhan, China. Her current research interests include wind turbine and VSC-HVDC control, small signal stability and interaction analysis of power electronized power systems.

Jiabing Hu received the B.Eng. and Ph.D. degrees from the College of Electrical Engineering, Zhejiang University, Hangzhou, China, in July 2004 and September 2009, respectively. From 2007 to 2008, he was funded by Chinese Scholarship Council as a Visiting Scholar with the Department of Electronic and Electrical Engineering, University of Strathclyde, Glasgow, U.K. From April 2010 to August 2011, he was a Postdoctoral Research Associate with Sheffield Siemens Wind Power Research Center and the Department of Electronic and Electrical Engineering, University of Sheffield, Sheffield, U.K. Since September 2011, he has been a Professor and now the Vice Dean of the State Key Laboratory of Advanced Electromagnetic Engineering and Technology, and the School of Electrical and Electronic Engineering, Huazhong University of Science and Technology, Wuhan, China. His current research interests include grid integration of large-scale renewables, modular multilevel converter for HVDC applications, and modeling, analysis, and control of power electronized power systems. He serves as an Editor for *IEEE Transactions on Energy Conversion* and *IEEE Power Engineering Letter*, an Associate Editor for *IET Renewable Power Generation*, and a member of Editorial Board for *Automation of Electric Power Systems*. He is the co-convenor of IEC SC8A JWG5 and the active expert of IEC SC8A WG1/AHG3. He was nominated in 2016 and 2019 by Elsevier to be between the most cited chinese researchers in electrical and electronic engineering.

Li Chai received the B.S. degree in Applied Mathematics and the M.S. degree in Control Science and Engineering from Zhejiang University, China, in 1994 and 1997, respectively, and the Ph.D degree in Electrical Engineering from the Hong Kong University of Science and Technology, Hong Kong, China, in 2002. From August 2002 to December 2007, he was at Hangzhou Dianzi University, China. He worked as a Professor at Wuhan University of Science and Technology, China, from 2008 to 2022. In August 2022, he joined Zhejiang University, China, where he is currently a Professor at the College of Control Science and Engineering. He has been a postdoctoral researcher or visiting scholar at Monash University, Newcastle University, Australia and Harvard University, USA. His research interests include stability analysis, distributed optimization, filter banks, graph signal processing, and networked control systems. Professor Chai is the recipient of the Distinguished Young Scholar of the National Science Foundation of China. He has published over 100 fully refereed papers in prestigious journals and leading conferences. He serves as the Associate Editor of *IEEE Transactions on Circuit and Systems II*: *Express Briefs, Control and Decision* and *Journal of Image and Graphs*.

Bing Liu received the Ph.D degree in Control Science and Engineering from Huazhong University of Science and Technology, Wuhan, China, in 2014. From September 2014 to December 2016, he was a Postdoctoral Fellow in the Department of Electrical and Computer Engineering, University of Windsor, Windsor, ON, Canada. He is currently an Associate Professor with the School of Information Science and Engineering, Wuhan University of Science and Technology, Wuhan. His research interests include distributed optimization and power systems.

Zixia Sang received the B.S., M.S., and Ph.D. degrees in Electrical Engineering from the Huazhong University of Science and Technology, Wuhan, China, in 2007, 2009, and 2014, respectively. He is currently with the Economic and Technology Research Institute, Hubei Electric Power Company. His research focuses on smart grid planning and design.